Recent decrease trend of atmospheric mercury concentrations in East China: the influence of anthropogenic emissions

Yi Tang[1, 2], Shuxiao Wang[1, 2*], Qingru Wu[1, 2*], Kaiyun Liu[1, 2], Long Wang[3], Shu Li[1], Wei Gao[4], Lei Zhang[5], Haotian Zheng[1, 2], Zhijian Li[1], Jiming Hao[1, 2]

[1] State Key Joint Laboratory of Environmental Simulation and Pollution Control, School of Environment, Tsinghua University, Beijing 100084, China

2 State Environmental Protection Key Laboratory of Sources and Control of Air Pollution Complex, Beijing 100084, China

3 School of Environment and Energy, South China University of Technology, Guangzhou, 510006, China

4 Yangtze River Delta Center for Environmental Meteorology Prediction and Warning, Shanghai, 20030, China

5 State Key Laboratory of Pollution Control & Resource Reuse, School of the Environment, Nanjing University, Nanjing, 210023, China

* *Correspondence to:* Shuxiao Wang (shxwang@tsinghua.edu.cn)

Qingru Wu (qrwu@tsinghua.edu.cn)

Abstract

Measurements of gaseous elemental Hg (GEM), other air pollutants including SO_2, NO_X, O_3, $PM_{2.5}$, CO, and meteorological conditions were carried out at Chongming Island in East China from March 1 in 2014 to December 31 in 2016. During the sampling period, GEM concentrations significantly decreased from 2.68±1.07 ng m^{-3} in 2014 (March to December) to 1.60 ±0.56 ng m^{-3} in 2016 (March to December). Monthly mean GEM concentrations showed a significant decrease with a rate of -0.60 ±0.08ng m^{-3} yr^{-1} (R^2=0.64, p<0.01 significance level). Combining the analysis of potential source contribution function (PSCF), principle component analysis (PCA), and emission inventory, we found that Yangtze River Delta (YRD) region was the dominant source region of GEM in Chongming Island and the main source industries included coal-fired power plants, coal-fired industrial boilers, and cement clinker production. We further quantified the effect of emission change on the air Hg concentration variations at Chongming Island through a coupled method of trajectory clusters and air Hg concentrations. It was found that the reduction of domestic emissions was the main driver of GEM decline in Chongming Island, accounting for 70% of the total decline. The results indicated that air pollution control policies targeting SO_2, NO_x and particulate matter reductions had significant co-benefits on GEM.

1 Introduction

Mercury (Hg) is of crucial concern to public health and the global environment for its neurotoxicity, long-distance transport, and bioaccumulation. The atmosphere is an important channel for global Hg transport. Once atmospheric Hg deposits to the aquatic system, it can be transformed into methylmercury (MeHg) which bio-accumulates through the food web and affects the central nervous system of human beings (Mason et al., 1995). Hg is therefore on the priority list of several international agreements and conventions dealing with environmental protection, including the *Minamata Convention on Mercury*.

Atmospheric Hg exists in three operationally defined forms: gaseous elemental mercury (GEM), gaseous oxidized mercury (GOM), and particulate-bound mercury (PBM). And the sum of GEM and GOM is known as total gaseous mercury (TGM). In the atmosphere, Hg mainly presents as GEM, accounting for over 95% of the total in the most observation sites (Fu et al., 2015; Li et al., 2016; Zhang et al., 2017). GEM is stable and with low solubility in the troposphere with a long residence time and can be transported at regional and global scale (Lindberg et al., 2007). GEM can be oxidized through photochemical reaction to GOM, which can be converted to PBM upon adsorption/absorption on aerosol surfaces. GOM is much soluble than GEM, and PBM can be quickly scavenged by both dry and wet deposition. Therefore, the residence time of both GOM and PBM is shorter than that of GEM, generally several days to a few weeks for GOM and 0.5 – 2 year for GEM (Schroeder and Munthe, 1998).

The atmospheric Hg observation results are important evidences to assess the effect of Hg emission control. During the past decades, significant decreases of GEM concentrations in Europe and North America have been observed (Cole et al., 2013; Weigelt et al., 2015). Air Hg concentrations in the northern hemisphere are reported to decline by 30-40% between 1990 and 2010 (Zhang Y et al., 2016). Such a decrease is consistent with the decrease in anthropogenic Hg emissions inventory in Europe and North America (Streets et al., 2011). So far, most of the long-term observations on the ground sites have been carried out in the developed countries. For the developing countries such as China, limited atmospheric Hg observations have been carried out (Fu et al., 2008b; Zhang H et al., 2016; Hong et al., 2016) and there is no official national

observing network of atmospheric Hg in mainland China. Therefore, there are few continuous multi-year observation records of China's air Hg concentrations published (Fu et al., 2015).

China contributes to the largest Hg emissions in the world and will continue to be one significant Hg emitter for global Hg emissions in the coming future (UNEP, 2013, Wu et al., 2016, Chen et al., 2018; Pacyna et al., 2016). Large Hg emissions in China have led to the average air Hg concentrations of 2.86 ± 0.95 ng m^{-3} (in the range of 1.60-5.07 ng m^{-3}) at the remote sites in China (Fu et al., 2015). Such Hg concentration level is approximately 1.3 ng m^{-3} higher than the background concentration of GEM in Northern Hemisphere (Zhang et al., 2016;Sprovieri et al., 2017;Fu et al., 2015). In addition, the large Hg emissions in China will also impact the air Hg concentrations in East Asia and even North America through long-range transport (Sung et al., 2018;Zhang et al., 2017). Meanwhile, China has a great potential for Hg emission reduction during implementation of the *Minamata Convention on Mercury* (Chen et al., 2018). Therefore, long-term atmospheric Hg observations in China are critical to understand the Hg cycling at both regional and global scale. China's Hg emissions had increased from 147 t yr^{-1} in 1978 to around 538 t yr^{-1} in 2010 due to the dramatic economic development (Zhang L et al., 2015; Wu et al., 2016; Hui et al., 2017). Atmospheric Hg monitoring that spanned the longest periods (from 2002 to 2010) in Guiyang, southwestern China witnessed the increase of Hg emissions in China (Fu et al., 2011). However, recently atmospheric Hg emissions in China have been estimated to decrease since 2012 (Wu et al., 2016). This decreasing trend needs to be confirmed by atmospheric Hg observations.

In this study, we measured GEM, other air pollutants (eg., $PM_{2.5}$ and NO_x), and meteorological parameters (eg., temperature and wind speed) at a remote marine site of Chongming Island in East China during 2014-2016. We analyzed annual and seasonal variation of GEM and the potential impact factors. Combining the analysis of potential source contribution function (PSCF), principle component analysis (PCA), and emission inventory, the potential source regions and source industries of atmospheric Hg pollution at the monitoring site are identified. In addition, a coupled trajectories and air Hg concentration method is developed to assess the effect of Hg emission change from different regions on air GEM concentration variation at the monitoring site.

2 Materials and methods

2.1 Site descriptions

The monitoring remote site (31°32′13″N, 121°58′04″E, about 10 m above sea level) locates at the top of weather station in Dongtan Birds National Natural Reserve, Chongming Island, China (Figure 1). As China's third largest island, Chongming Island is located in the east of Yangtze River Delta region with a typical subtropical monsoon climate. It is rainy, hot, with southern and southeastern winds in summer and is dry, cold, and with northwestern wind in winter. The dominant surface types are farmland and wetland. There are no large anthropogenic emission sources in the island and no habitants within 5 km distance from the site. The downtown Shanghai area is 50 km to the southwest of the site.

2.2 Sampling methods and analysis

During the monitoring period, we used Tekran 2537X/1130/1135 instruments to monitor speciated Hg in the atmosphere, which was widely used for air Hg observation in the world. The sampling inlet was 1.5 m above the instrument platform. Continuous 5-minute of GEM was measured by Tekran 2537X Hg vapor analyzer with the detection limit of 0.1 ng m^{-3} at a sampling flow rate of 1.0 L min^{-1} during two campaigns: March 1, 2014 to December 31, 2015 and March 26 to December 31, 2016. From July 5, 2015 to April 30 2016, the Tekran 1130/1135 speciation unit was damaged by the rainstorm, the Tekran 2537X were operated without speciation units but with PTFE filter to protect the instrument from particles and sea salt. Therefore, the observed concentrations during July 2015-April 2016 were TGM concentrations indeed. However, the GOM concentrations at Chongming Island accounted for less than 1% of TGM (TGM=GOM+GEM). Thus, the GEM concentrations were approximated to TGM concentrations from July 2015 to April 2016.

The 2537X analyzer was calibrated automatically every 25 h using the internal Hg permeation source inside the instrument, and the internal permeation source was calibrated every 12 months with manual injection of Hg by a syringe from an external Hg source (module 2505). Two zero and two span calibrations were performed for each calibration of gold trap A and B, respectively. The difference between gold trap A and gold trap B was limited to ±10 %. The impactor plates and

quartz filter were changed in every two weeks. The soda lime was changed once a month. The denuders were recoated once every two weeks following the procedure developed by Landis et al. (2002).

In our research, random uncertainties of individual measurement had been averaged out and the systematic uncertainties need to be considered. The overall practically achievable systematic uncertainty would be 10% considering that the instrument was not in ideal performance (Slemr et al., 2015; Steffen et al., 2012). For example, slow deactivation of the traps, contamination of the switching valves and leaks would increase the uncertainties but were difficult to quantify (Slemr et al., 2015;Steffen et al., 2012). Because of the consistency of instrument and the quality assurance/quality control have been paid special attention to during the sampling campaign, the systematic differences of instrument did not affect the huge variation between 2014 and 2016.

During the sampling campaigns, $PM_{2.5}$, O_3, NO_x, CO and SO_2 were also monitored by Thermo Scientific TEOM 1405D, Model 49i O_3 Analyzer, Model 48i CO Analyzer, Model 42i-TL NOx Analyzer and Model 43i SO_2 Analyzer, respectively. The detection limits of O_3, SO_2, NO_x, CO and $PM_{2.5}$ are 1.0, 0.5, 0.4, 0.04 and 0.1 μg m^{-3}, respectively. The meteorological parameters including air temperature, wind speed, and wind direction are measured by Vantage Pro2 weather station (Davis Instruments). The instruments are tested and calibrated periodically. All data are hourly averaged in this study.

2.3 Sources apportionment of atmospheric Hg pollution

2.3.1 PSCF model

To identify the source areas for pollutants with a relatively long lifetime such as GEM (Xu and Akhtar, 2010), the PSCF values for mean GEM concentrations in grid cells in a study domain are calculated by counting the trajectory segment endpoints that terminate within each cell. The number of endpoints that fall in the *ij*-th cell are designated n_{ij}. The number of endpoints for the same cell having arrival times at the monitoring site corresponding to GEM concentrations higher than a specific criterion is defined to be m_{ij}. The criterion in this study is set as the average Hg concentration during our study period. The PSCF value for the *ij*-th cell is then defined as:

$$PSCF_{ij} = \frac{m_{ij}}{n_{ij}} W_{ij} \quad (1)$$

where W_{ij} is an empirical weight to reduce the effects of grid cells with small n_{ij} values. In this study, W_{ij} is defined as in the following formula, in which Avg is the mean n_{ij} of all grid cells with n_{ij} greater than zero:

$$W_{ij} = \begin{cases} 1.0 & n_{ij} > 2 * Avg \\ 0.7 & Avg < n_{ij} \leq 2 * Avg \\ 0.42 & 0.5 * Avg < n_{ij} \leq Avg \\ 0.17 & n_{ij} \leq 0.5 * Avg \end{cases} \quad (2)$$

The PSCF value indicates the probability of a grid cell through which polluted events occurs. More method details can be found in the study of Polissar et al. (Polissar et al., 1999). In this study, the domain that covered the potential contribution source region (105 °–135 °E, 15 °–45 °N) was divided into 22500 grid cells with 0.2 ° ×0.2 °resolution. 72-hour back trajectories were generated hourly from 1 March, 2014 to 31 December, 2015 and from March 26 to December 31 in 2016 by TrajStat, a software including HYSPLIT for trajectory calculation with trajectory statistics modules (Wang et al., 2009). PSCF map was plotted using ArcGIS version 10.1.

2.3.2 Principal component analysis (PCA)

Correlation between Hg and other pollutant concentrations are used to identify source industries. Strong positive loadings (loading>0.40) with SO_2 and $PM_{2.5}$ typically indicate the impact of coal combustion, and strong positive loadings with GEM and CO have often been used as an indicator for regional transport because both pollutants have similar source and stable chemical properties (Lin et al., 2006; Pirrone et al., 1996). In this study, PCA was applied to infer the possible influencing factors of GEM in 2014 and 2016. Prior to analysis, each variable was normalized by dividing its mean, and pollutant concentrations (SO_2, CO, NO_X, $PM_{2.5}$) were averaged to 1-h sampling intervals to match the hourly Hg monitoring during sampling period. The results in 2016 had no CO data due to instrument broken. Statistics analyses were carried out by using SPSS 19.0 software.

2.4 Quantification method of source contribution

To further quantitatively assess the effect of change in emissions from different regions on air concentrations variation at a certain monitoring site, a quantitative estimation method which coupled trajectories with air Hg concentrations was developed. We firstly identified the trajectories by using the National Oceanic and Atmospheric Administration (NOAA) Hybrid Single-Particle Lagrangian Integrated Trajectory (HYSPLIT) model. The gridded meteorological

177 data at a horizontal resolution of 1 °×1 °were obtained from the Global Data Assimilation System
178 (GDAS) (Draxler and Hess, 1998). The starting heights were set to be 500 m above ground level
179 to represent the center height of boundary layer where pollutants are usually well mixed in
180 boundary layer. Secondly, each trajectory was assigned with GEM concentration by matching the
181 arriving time in Chongming site. Third, the backward trajectories which coupled with Hg
182 concentrations were clustered into groups according to transport patterns by using NOAA
183 HYSPLIT 4.7. Thus, the grouped clusters were applied to identify the Hg source regions. The Hg
184 average concentration of the cluster *j* was then calculated as equation (3). And, the trajectory
185 weighted concentration in the cluster *j* as equation (4). At last, the contribution of reduction at a
186 certain region on Hg concentration at monitoring sites in a certain period can be calculated as
187 equation (5).
188

189 $$C_{j,t} = \frac{\sum_{i=1}^{n} C_{i,j,t}}{\sum_{i=1}^{n} N_{i,j,t}} \quad (3)$$

190 $$TWC_{j,t} = AR \times C_{j,t} \quad (4)$$

191 where *N* refers to a certain trajectory. *j* refers to a certain cluster. *t* is the studied period, and *n* is
192 the number of trajectory. *m* is the number of cluster. *C* is the GEM concentration, ng m^{-3}. *TWC*
193 refers to the trajectory weighted concentration, ng m^{-3}. In order to reduce the influence of
194 trajectory changes in different region between calculated years, the average ratio (AR) was used
195 here for calculating TWC.

196 $$CR_j = \frac{TWC_{j,t_2} - TWC_{j,t_1}}{\sum_{j=1}^{m} TWC_{j,t_2} - \sum_{j=1}^{m} TWC_{j,t_1}} \quad (5)$$

197 where *CR* refers to the contribution of GEM reduction. t_1 and t_2 refers to the two period
198 participating to comparison, namely year 2014 and 2016 in this study, respectively.
199 This approach is a simple method to quantify the influence of anthropogenic emissions on GEM
200 concentration variation. It should be noted that uncertainties always exist in calculating
201 trajectories, causing uncertainties in all trajectory-based approaches. Trajectory errors vary

considerably in different situation. Draxler (1996) suggested uncertainties might be 10% of the travel distance. Besides, meteorological conditions were pretty similar in 2014 and 2016 so as to reduce the interference from meteorology (Table S2).

2.5 Regional atmospheric Hg emissions

Regional anthropogenic GEM emissions by month are calculated by using both the technology-based emission factor methods and transformed normal distribution function method. Detailed introduction of these two methods and the speciation profile of the emitted Hg for each sector are described in our previous study (Wu et al., 2016). Conventional air pollutant (SO_2, $PM_{2.5,}$ and NO_x) emissions were calculated following the study of Zhao et al. (2013). The source regions included in the emission inventory consisted of Shanghai, Jiangsu, Zhejiang, and Anhui provinces according to the PSCF results (See section 3.3). The studied emission sectors included coal-fired power plants, coal-fired industrial boilers, residential coal-combustion, cement clinker production, iron and steel production, mobile oil combustion and other small emission sectors (eg., zinc smelting, lead smelting, municipal solid incineration, copper smelting, aluminum production, gold production, other coal combustion, stationary oil combustion, and cremation). The monthly Hg emissions were mainly distributed according to fuel combustions or products productions by month (Table S1). For small emission sectors, the annual emissions were equally distributed into monthly emissions. The GEM emissions from natural sources E_N are calculated as followings.

$$E_N = \sum_i F_i \times A_i \times t \quad (6)$$

where F_i is a bi-directional Hg flux of canopy i, ng km^{-2} yr^{-1}; A is the studied area, km^{-2}; t is the studied year, yr. The bi-directional Hg flux was obtained from the study of Wang et al. (2016) directly. It should be pointed out that the natural emission is a concept of net emission in this manuscript, which reflected a net effect of two competing processes (Zhang, 2009): total Hg natural emissions and total Hg deposition. The total natural emissions included primary natural release and re-emission of legacy Hg stored in the terrestrial and water surface (Wang et al., 2016). When the value is positive, it means the net effect is Hg emissions to air. Otherwise, Hg deposited.

3 Results and discussions

3.1 Decreasing trends of atmospheric Hg during 2014-2016

The average concentrations of GEM in 2014 (March to December), 2015 and 2016 (March to December) were 2.68±1.07 ng m^{-3}, 2.14 ± 0.82 ng m^{-3}, and 1.60±0.56 ng m^{-3}, respectively. The GEM concentrations in 2014 were higher (*t* test, $p<0.01$) than the Northern Hemisphere back-ground concentration (about 1.5 ng m^{-3}) (Sprovieri et al., 2010) and those measured in other remote and rural locations in China (Zhang H et al., 2015; Fu et al., 2008a; Fu et al., 2009). However, in 2016, the GEM concentrations were similar to the background concentrations in the Northern Hemisphere. During this period, monthly GEM concentrations showed a significant decrease with a rate of -0.60 ± 0.08 ng m^{-3} yr^{-1} (R^2=0.64, p<0.01 significance level, n = 32) (Figure 2a). The amount of valid data for each mouth was shown in Table S3. From another aspect, the trend decomposition of the GEM concentration signal (signal = trend + seasonal + random) from March 2014 to December 2016 were performed in Figure 2 (https://anomaly.io/seasonal-trend-decomposition-in-r/). By using this method, we also observed a pronounced trend (Figure 2b) and the random was limited in the range of -0.24 – 0.24 ng m^{-3} (Figure 2d).

One potential worry is that the calculated trend will be sensitive to seasonal variation and the missing data in January and February of 2016 may impact the downward trend. To evaluate the impact of the missing data, we estimate the Hg concentrations in the missing months based on the data of the same months in 2015 and 2017 (Figure S1). Combining the estimated data, we re-fit the Hg concentrations and downward trend still maintained robust and similar to the downward trend in manuscript (Figure S1). Thus, we assume that the missing data is not very important and will not impact our main conclusion.

Table S4 showed the Hg variation trends in different regions. Significant decreases of GEM concentrations in North hemisphere over the past two decades have been well documented (Weigelt et al., 2015; Cole et al., 2013; Kim et al., 2016). All the stations in Table S4 used Tekran instruments except for the observation in South Korea. Different instruments could cause potential differences in the observation, but they were comparable and did not affect the conclusion of

comparison in downward trend (Slemr et al., 2015; Sprovieri et al., 2016). Weigelt et al. (2015) showed that GEM concentrations decreased from 1.75 ng m^{-3} in 1996 to 1.4 ng m^{-3} in 2009 at Mace Head, Europe. Ten-year trends of GEM concentrations at six ground-based sites in the Arctic and Canada also showed a decreasing trend at a rate of 13-35 pg m^{-3} y^{-1} (Cole et al., 2013). In South Korea, the observed GEM concentration also had significant decrease in recent years (Kim et al., 2016). In South Africa, annual average GEM concentration at Cape Point decreased from 1.29 ng m^{-3} in 1996 to 1.19 ng m^{-3} in 2004 (Slemr et al., 2008) and were increasing from 0.93 ng m^{-3} in 2007 (Slemr et al., 2015) until 2016 (Martin et al, 2017). However, limited GEM monitoring sites and relative short-time spans in China restricted the views of long-term trends in atmospheric Hg concentration in this region. A preliminary assessment indicated that atmospheric Hg concentrations in China kept increasing before 2012 (Fu et al., 2015). The decreasing trend observed in our study was accordant with reported data in Mt. Changbai during 2014-2015 cited in the review of Fu et al. (2015). The atmospheric Hg at Chongming was influenced by and in turn reflected regional Hg emission and cycle. Although the decline in atmospheric Hg was observed in many sites of the Northern Hemisphere, much sharper decrease of Hg concentrations was observed at Chongming in our study. The specific reasons for the Hg concentration decrease in our study will be discussed in section 3.4.

3.2 Seasonal variation of GEM concentrations

According to the decomposition result (Figure 2c), we observed strong seasonal cycle with seasonal GEM peak in July and trough in September, so GEM concentrations in the same month but different years were averaged to discuss the seasonal circle (Figure 3). The average data can eliminate the effect of downward trend and get result of average seasonal variation. The error bars in the Figure 3 mean the standard deviation of the monthly average. Observed GEM concentrations showed an obvious seasonal cycle. The mean GEM concentration in warm season (from April to September) is 0.29 ng m^{-3} higher than that in cold season. Such seasonal variation trend is also observed at Nanjing, Miyun, Mt. Ailao, Mt. Waliguan, and Shangri-La (Zhang et al., 2013; Zhang et al., 2016; Fu et al., 2015; Zhu et al., 2012). On the other hand, the means of GEM at Mt. Gongga, Mt. Daimei, Mt.Leigong, and Mt. Changbai in China are relatively higher in cold seasons. The average of atmospheric Hg concentrations in the north hemisphere also have a trough

value in summer (Sprovieri et al., 2016).

Seasonal variations of GEM concentration are generally attributed to the following factors, including natural and anthropogenic emissions, atmospheric chemical reaction, and air mass transportation. The higher Hg concentrations in cold seasons in Mt. Leigong were mainly explained by coal-combustion for urban and residential heating during cold seasons. Whereas, increasing solar radiation and soil/air temperature dominate the higher Hg concentrations in Mt. Ailao. In addition, sites in southern, eastern, and northeastern China also impacted from anthropogenic emissions of GEM from the north and west by the northerly winter monsoon while the sites located in western, southwestern, and northern China were impacted in the warm season (Fu et al., 2015). As to most sites in the northern hemisphere, high wet Hg precipitation induced probably by faster GEM oxidation led to lower Hg concentrations in summer.

Source emission is one significant factor on GEM concentrations in the air. The GEM concentrations at a remote site are generally regarded under the impact of regional emissions. Therefore, the emissions in the YRD regions (Anhui, Zhejiang, Jiangsu, and Shanghai) were calculated. However, the anthropogenic emissions were in the range of 2.5-2.7 t, which is almost unchanged. Compared to the anthropogenic emissions, we observed almost synchronized trends between natural emissions and air Hg concentrations in Figure 4. The natural emissions showed a huge seasonal variation, from -5.4 t to 8.4 t. The largest natural emissions were observed in summer when the highest GEM concentrations were monitored. In the autumn, the natural emissions performed as the largest deposition direction amount and the GEM concentrations were the lowest in the whole year. Therefore, natural emissions instead of anthropogenic were supposed to be one significant factor of the seasonal cycle of GEM concentrations (Figure 4). The seasonal trend of natural emissions is closely related with the canopy types in YRD areas, where widely subtropical forests, paddy field, and dry farming were observed (Figure S2). The high temperature will speed up decomposition of organic compound in soil, which leads to Hg emissions from farmland and forest in YRD region (Luo et al., 2016; Yu et al., 2017). In autumn and winter, with the decrease of temperature (Table S2), the role of soil changed from Hg source to sink, which reduces the Hg concentrations in the air (Wang et al., 2016). At the same time, the growing vegetation in autumn also absorbs air Hg, resulting lower Hg concentrations compared to that in

winter. Transport also overall enhanced the observed seasonal variation of GEM concentrations at Chongming Island. According to the statistics of backward trajectories in section 3.4, the GEM concentrations in the air mass which did not pass via the YRD regions also showed high GEM concentration in warm season in 2014 (Figure S3).

From Figure 2, we also observed more pronounced seasonal variation in 2014, which can be attributed to the lower wet deposition and GEM oxidation. On one aspect, as a costal site, the Chongming Island is abundant with •OH. The increase of O_3 concentration from the summer of 2014 to 2016 may contribute to a higher oxidation of GEM in 2016. On another aspect, and higher wet Hg deposition is approximately 6.6 times of that in the winter at Chongming (Zhang et al., 2010). Meanwhile, the rainfall in 2016 summer (546 mm) was higher than the rainfall in 2014 (426 mm). Therefore, the higher oxidation and wet deposition rate of Hg in the summer of 2016 will reduce the concentration difference between summer and winter, which lead to a less pronounced seasonal variation in 2016. Meanwhile, the higher oxidation and wet deposition in 2016 also contributed to the downward trend of GEM by reducing the seasonality in spring and summer (Figure S3).

3.3 Source apportionment of atmospheric Hg pollutions

According to the PSCF result, YRD region, including Shanghai, Jiangsu, Anhui, and Zhejiang provinces, was the dominant source region in both 2014 and 2016 (Figure 5). Therefore, Hg emissions from these areas would contribute to high proportion of Hg pollution at Chongming Island. The offshore area mainly around Jiangsu province also has a high PSCF value because some trajectories from North China, especially Shandong province, transport to Chongming Island through this area. Compared to the result in 2014, the PSCF value had an obvious decline in East China Sea in 2016. The decline from the East China Sea may be contributed by the downward trend of GEM concentrations in South Korea and Japan (Kim et al., 2016; Kim et al., 2013), where the anthropogenic Hg emissions of Japan and South Korea have been reduced by 13% and 4% during 2010-2015, respectively (UNEP 2013; UNEP 2018). The air mass from Japan and South Korea would pass through the East China Sea to Chongming.

PCA method was applied to preliminarily identify the source industries. In the studied period, totally 2 factors were identified in 2014 and 2016, respectively. The factor 1 had strong factor

loadings of GEM, SO_2, NO_x, CO, and $PM_{2.5}$ in both 2014 and 2016 (No CO data in 2016 due to equipment problems). The factor 1 accounted for 49% variance in 2014 and 50% variance in 2016 (Table 1). The results indicated common significant source sectors of the above five air pollutants, which can also be proven from emission inventories (Table 2). The dominant source industries included coal-fired power plants, coal-fired industrial boilers, and cement clinker production. The PCA results showed that anthropogenic emissions were the main sources of GEM during the sampling period.

The factor 2 in both 2014 and 2016 had a strong positive loading on O_3 and negative loading on NO_x. Considering the low loading of CO and high loading of O_3, the factor 2 can be viewed as a sign of the invasion of air mass from stratosphere (Fishman and Seiler, 1983; Jaffe, 2010). The air mass from stratosphere will increase the O_3 concentration. O_3 react with NO, which makes a negative correlation with NO. However, the low loading on GEM of factor 2 indicated that Factor 2 had no relationship with GEM concentrations at Chongming from the aspect of whole year data.

3.4 The influence of anthropogenic emissions

To further understand the reason of the downward trend, we firstly compared the meteorological conditions in both 2014 and 2016. We noted that the difference of annual temperature, solar radiation, and relative humidity were constrained in the range of 17.13±7.48 ℃, 165.55±45.87 W m^{-2} and 75.38±5.82%, respectively (Table S2). The coefficient of variation for annual mean of these meteorological conditions in 2014 and 2016 was 2.6%, 6.7% and 0.2%, respectively. In addition, the wind rose was similar, and the dominating wind was from SE in both 2014 and 2016 (Figure S4). The HYSPLIT results also provided similar trajectories in 2014 and 2016 (Figure 6). Therefore, we assumed that the meteorological condition was not the dominant reason of GEM decline at Chongming site.

To further quantify the driver of GEM decline, a trajectory-based analysis method was used in this study. The 72-h air mass back trajectories were calculated using HYSPLIT for every 8 hours starting at the observation site. Approximately 918 and 832 trajectories were calculated in sampling period in 2014 (Mar 1 to Dec 31, 2014) and 2016 (Mar 26 to Dec 31, 2016), respectively. The trajectories were grouped into 3 clusters in each year according to geographical regions (Figure 6). The first cluster of trajectories mainly passed through the regions (eg., North China)

north and northwest to Chongming Island before arriving to our monitoring site, which was denoted as cluster NCP. The second cluster mainly passed YRD region to Chongming, which was signed as cluster SW-YRD. The third type mainly originated from the East China Seas, South Korea, Japan and Northeast Asia continent, and then arrived to our monitoring sites directly without passing the mainland China. This type of trajectories was named as cluster ABROAD. Some trajectories originated from the East China Sea and crossed the mainland China before arriving Chongming were grouped into cluster NCP or SW-YRD depending on the regions it crossed. The trajectories for each of the three clusters in 2014 and 2016 were shown in Table 3.

Table 3 showed the detail statistics data of the three classifications. From 2014 to 2016, the whole China region (NCP, SW-YRD) contributed to 70% of GEM decline at Chongming Island. Considering downward trend of emission inventory and atmospheric pollutant from 2014 to 2016 in NCP and SW-YRD region (Table S5, Table S6), the reason of downward trend can be attributed to the effectiveness of existing air pollution control measures in China (SC, 2013; MEP, 2014). Meanwhile, the cluster NCP, cluster SW-YRD, and cluster ABROAD caused 26%, 44%, and 30% for GEM decline, respectively (Table 3). The cluster SW-YRD contributed to 44% of reduction, suggesting that air pollution controls on anthropogenic emissions in YRD region dominated the recent decrease of GEM concentrations at Chongming site. The largest decline of Hg concentration (1.32 ng m^{-3}) was also observed in the cluster SW-YRD demonstrated the efficiency of emission reduction in YRD region (Table S5, Table S6). Moreover, ABROAD region caused 30% of GEM decline from 2014 to 2016, which implies global effort on atmospheric Hg emission control under the guidance of *Minamata Convention on Mercury*.

4 Conclusion

Atmospheric Hg was continuously measured for three years at a regional background site in the YRD region. During the sampling period, a downward trend for GEM concentrations (-0.60 ± 0.08 ng m^{-3} y^{-1}) at Chongming Island was observed. The seasonal GEM cycle was dominated by the natural emissions while the annual GEM concentration trend was mainly impacted by anthropogenic emissions. By using a new approach that considers both cluster frequency and the Hg concentration associated with each cluster, we quantified that atmospheric Hg from NCP

region, SW-YRD region, and ABROAD region have caused 26%, 44%, and 30% decline of GEM concentrations at Chongming monitoring site, respectively. The result suggested that reduction of anthropogenic emissions in mainland China was the main cause of the recent decreasing trend of GEM concentration at Chongming site. The air pollution control policies in China, especially the pollution control in the coal-fired power plants, coal-fired industrial boilers, and cement clinker production in YRD region and Shandong province, have received significant co-benefit of atmospheric Hg emission reductions. On the other hand, emission reduction from the ABROAD region, where clusters arrived to Chongming monitoring site directly without passing the mainland China, implies global effort on atmospheric Hg emission control under the guidance of *Minamata Convention on Mercury*. Considering that the *Minamata Convention on Mercury* had come into force in 2017, continuous long-term observation of atmospheric Hg in China will be required for the assessment of policy effectiveness.

Data availability. All data are available from the authors upon request.

Competing interests. The authors declare that they have no conflict of interest.

Acknowledge. This work is sponsored by the Natural Science Foundation of China (No. 21607090), Major State Basic Research Development Program of China (973 Program) (No. 2013CB430000), National Key R&D Program of China (No. 2016YFC0201900)

References

Cole, A. S., Steffen, A., Pfaffhuber, K. A., Berg, T., Pilote, M., Poissant, L., Tordon, R., and Hung, H.: Ten-year trends of atmospheric mercury in the high Arctic compared to Canadian sub-Arctic and mid-latitude sites, Atmospheric Chemistry and Physics, 13, 1535-1545, 2013.

Chen, L., Zhang, W., Zhang, Y., Tong, Y., Liu, M., Wang, H., Xie, H., and Wang, X.: Historical and future trends in global source-receptor relationships of mercury, Science of the Total Environment, 610-611, 24-31, 2018.

Draxler, R. R.: Trajectory Optimization for Balloon Flight Planning, International Journal for Numerical Methods in Fluids, 5, 13-23, 1996.

Draxler, R. R., and Hess, G. D.: An overview of the hysplit-4 modeling system for trajectories, Australian Meteorological Magazine, 47, 295-308, 1998.

Fishman J, Seiler W. Correlative Nature of Ozone and Carbon Monoxide in the Troposphere: Implications for the Tropospheric Ozone Budget. Journal of Geophysical Research, 88(C6), 1983.

Fu, X. W., Feng, X. B, Zhu, W. Z., Wang, S. F., and Lu, J. L.: Total gaseous mercury concentrations in ambient air in the eastern slope of Mt. Gongga, South-Eastern fringe of the Tibetan plateau, China, Atmospheric Environment, 42, 970-979, 2008a.

Fu, X. W., Feng, X. B., Zhu, W. Z., Zheng, W., Wang, S. F., and Lu, J. Y.: Total particulate and reactive gaseous mercury in ambient air on the eastern slope of the Mt. Gongga area, China, Applied Geochemistry, 23, 408-418, 2008b.

Fu, X. W., Feng, X. B., Wang, S., Rothenberg, S., Shang, L., Li, Z., and Qiu, G.: Temporal and spatial distributions of total gaseous mercury concentrations in ambient air in a mountainous area in southwestern China: implications for industrial and domestic mercury emissions in remote areas in China, Science of the Total Environment, 407, 2306-2314, 2009.

Fu, X. W., Feng, X. B., Qiu, G. L., Shang, L. H., and Zhang, H.: Speciated atmospheric mercury and its potential source in Guiyang, China, Atmospheric Environment, 45, 4205-4212, 2011.

Fu, X. W., Zhang, H., Yu, B., Wang, X., Lin, C. J., and Feng, X. B.: Observations of atmospheric mercury in China: a critical review, Atmospheric Chemistry and Physics, 15, 9455-9476, 2015.

Hong, Q. Q., Xie, Z. Q., Liu, C., Wang, F. Y., Xie, P. H., Kang, H., Xu, J., Wang, J. C., Wu, F. C.,

He, P. Z., Mou, F. S., Fan, S. D., Dong, Y. S., Zhan, H. C., Yu, X. W., Chi, X. Y., and Liu, J. G.: Speciated atmospheric mercury on haze and non-haze days in an inland city in China, Atmospheric Chemistry and Physics, 16, 13807-13821, 2016.

Hui, M. L., Wu, Q. R., Wang, S. X., Liang, S., Zhang, L., Wang, F. Y., Lenzen, M., Wang, Y. F., Xu, L. X., Lin, Z. T., Yang, H., Lin, Y., Larssen, T., Xu, M., and Hao, J. M.: Mercury flows in China and global drivers, Environmental Science & Technology, 51, 222-231, 2017.

Jaffe, D.: Relationship betwen surface and free tropospheric ozone in the western U.S., Environmental Science & Technology, 45, 432-438, 2010.

Kim, K.-H., Yoon, H.-O., Brown, R. J. C., Jeon, E.-C., Sohn, J.-R., Jung, K., Park, C.-G., and Kim, I.-S.: Simultaneous monitoring of total gaseous mercury at four urban monitoring stations in Seoul, Korea, Atmospheric Research, 132-133, 199-208, 2013.

Kim, K. H., Brown, R. J. C., Kwon, E., Kim, I. S., and Sohn, J. R.: Atmospheric mercury at an urban station in Korea across three decades, Atmospheric Environment, 131, 124-132, 2016.

Landis, M. S., Stevens, R. K., Schaedlich, F., and Prestbo, E. M.: Development and characterization of an annular denuder methodology for the measurement of divalent inorganic reactive gaseous mercury in ambient air, Environmental Science & Technology, 36, 3000-3009, 2002.

Lindberg, S., Bullock, R., Ebinghaus, R., Engstrom, D., Feng, X. B., Fitzgerald, W., Pirrone, N., Prestbo, E., and Seigneur, C.: A synthesis of progress and uncertainties in attributing the sources of mercury in deposition, Ambio, 36, 19, 2007.

Li, S., Gao, W., Wang, S. X., Zhang, L., Li, Z. J., Wang, L., and Hao, J. M.: Characteristics of Speciated Atmospheric Mercury in Chongming Island, Shanghai, Environmental Science 37, 3290 - 3299, 2016.

Luo, Y., Duan, L., Driscoll, C. T., Xu, G., Shao, M., Taylor, M., Wang, S. X, and Hao, J. M.: Foliage/atmosphere exchange of mercury in a subtropical coniferous forest in south China, Journal of Geophysical Research Biogeosciences, 121, 2016.

Martin, L. G., Labuschagne, C., Brunke, E. G., Weigelt, A., Ebinghaus, R., and Slemr, F.: Trend of atmospheric mercury concentrations at Cape Point for 1995–2004 and since 2007, Atmospheric Chemistry and Physics, 17, 2393-2399, 2017.

Mason, R. P., Reinfelder, J. R., and Morel, F. M. M.: Bioaccumulation of mercury and methylmercury, Springer Netherlands, 915-921 pp., 1995.

Ministry of Environmental Protection (MEP) and State Administration for Quality Supervision and Inspection and Quarantine (AQSIQ): Emission standard of air pollutants for boilers, MEP, Beijing, China, 2014.

Pirrone, N., Keeler, G. J., and Nriagu, J. O.: Regional differences in worldwide emissions of mercury to the atmosphere, Atmospheric Environment, 30, 2981-2987, 1996.

Polissar, A. V., Hopke, P. K., Paatero, P., Kaufmann, Y. J., Hall, D. K., Bodhaine, B. A., Dutton, E. G., and Harris, J. M.: The aerosol at Barrow, Alaska: long-term trends and source locations, Atmospheric Environment, 33, 2441-2458, 1999.

State Council of the People's Republic of China (SC): Action plan of national air pollution prevention and control, SC, Beijing, China, 2013.

Schroeder, W. H., and Munthe, J.: Atmospheric mercury—An overview, Atmospheric Environment, 32, 809-822, 1998.

Slemr, F., Angot, H., Dommergue, A., Magand, O., Barret, M., Weigelt, A., Ebinghaus, R., Brunke, E. G., Pfaffhuber, K. A., Edwards, G., Howard, D., Powell, J., Keywood, M., and Wang, F.: Comparison of mercury concentrations measured at several sites in the Southern Hemisphere, Atmospheric Chemistry and Physics, 15, 3125-3133, 2015.

Sprovieri, F., Pirrone, N., Ebinghaus, R., Kock, H., and Dommergue, A.: A review of worldwide atmospheric mercury measurements, Atmospheric Chemistry and Physics, 10, 8245-8265, 2010.

Streets, D. G., Devane, M. K., Lu, Z., Bond, T. C., Sunderland, E. M., and Jacob, D. J.: All-Time releases of mercury to the atmosphere from human activities, Environmental Science & Technology, 45, 10485-10491, 2011.

Sprovieri, F., Pirrone, N., Bencardino, M., amp, apos, Amore, F., Carbone, F., Cinnirella, S., Mannarino, V., Landis, M., Ebinghaus, R., Weigelt, A., Brunke, E.-G., Labuschagne, C., Martin, L., Munthe, J., Wängberg, I., Artaxo, P., Morais, F., Barbosa, H. d. M. J., Brito, J., Cairns, W., Barbante, C., Diéguez, M. d. C., Garcia, P. E., Dommergue, A., Angot, H., Magand, O., Skov, H., Horvat, M., Kotnik, J., Read, K. A., Neves, L. M., Gawlik, B. M., Sena, F., Mashyanov, N., Obolkin, V., Wip, D., Feng, X. B., Zhang, H., Fu, X., Ramachandran, R., Cossa, D., Knoery, J.,

Marusczak, N., Nerentorp, M., and Norstrom, C.: Atmospheric mercury concentrations observed at ground-based monitoring sites globally distributed in the framework of the GMOS network, Atmospheric Chemistry and Physics, 16, 11915-11935, 2016.

Sprovieri, F., Pirrone, N., Bencardino, M., amp, apos, Amore, F., Angot, H., Barbante, C., Brunke, E.-G., Arcega-Cabrera, F., Cairns, W., Comero, S., Diéguez, M. d. C., Dommergue, A., Ebinghaus, R., Feng, X. B., Fu, X., Garcia, P. E., Gawlik, B. M., Hageström, U., Hansson, K., Horvat, M., Kotnik, J., Labuschagne, C., Magand, O., Martin, L., Mashyanov, N., Mkololo, T., Munthe, J., Obolkin, V., Ramirez Islas, M., Sena, F., Somerset, V., Spandow, P., Vardè, M., Walters, C., Wängberg, I., Weigelt, A., Yang, X., and Zhang, H.: Five-year records of mercury wet deposition flux at GMOS sites in the Northern and Southern hemispheres, Atmospheric Chemistry and Physics, 17, 2689-2708, 2017

Steffen, A., Scherz, T., Olson, M., Gay, D., and Blanchard, P.: A comparison of data quality control protocols for atmospheric mercury speciation measurements, J Environ Monit, 14, 752-765, 2012.

Sung, J.-H., Roy, D., Oh, J.-S., Back, S.-K., Jang, H.-N., Kim, S.-H., Seo, Y.-C., Kim, J.-H., Lee, C. B., and Han, Y.-J.: Trans-boundary movement of mercury in the Northeast Asian region predicted by CAMQ-Hg from anthropogenic emissions distribution, Atmospheric Research, 203, 197-206, 2018.

Arctic Monitoring and Assessment Programme and United Nations Environment Programme (AMAP/UNEP): Global Hg assessment 2013: sources, emissions, releases and environmental transport, AMAP/UNEP, Geneva, Switzerland, 2013

Arctic Monitoring and Assessment Programme and United Nations Environment Programme (AMAP/UNEP): Global mercury assessment 2018 - draft technical background document, AMAP/UNEP, Geneva, Switzerland, 2018.

Wang, X., Lin, C.-J., Yuan, W., Sommar, J., Zhu, W., and Feng, X.: Emission-dominated gas exchange of elemental mercury vapor over natural surfaces in China, Atmospheric Chemistry and Physics, 16, 11125-11143, 2016.

Wang, Y. Q., Zhang, X. Y., and Draxler, R. R.: TrajStat: GIS-based software that uses various trajectory statistical analysis methods to identify potential sources from long-term air pollution measurement data, Elsevier Science Publishers B. V., 938-939 pp., 2009.

Weigelt, A., Ebinghaus, R., Manning, A. J., Derwent, R. G., Simmonds, P. G., Spain, T. G., Jennings, S. G., and Slemr, F.: Analysis and interpretation of 18 years of mercury observations since 1996 at Mace Head, Ireland, Atmospheric Environment, 100, 85-93, 2015.

Wu, Q., Wang, S., Li, G., Liang, S., Lin, C. J., Wang, Y., Cai, S., Liu, K., and Hao, J.: Temporal trend and spatial distribution of speciated atmospheric mercury emissions in China during 1978-2014, Environmental Science & Technology, 50, 13428-13435, 2016.

Xu, X., and Akhtar, U. S.: Identification of potential regional sources of atmospheric total gaseous mercury in Windsor, Ontario, Canada using hybrid receptor modeling, Atmospheric Chemistry and Physics, 10, 7073-7083, 2010.

Yu Q, Luo Y, Wang S, Wang Z, Hao J, Duan L. Gaseous Elemental Mercury (GEM) Fluxes over Canopy of Two Typical Subtropical Forests in South China. Atmospheric Chemistry and Physics, 18(1), 495-509, 2018.

Zhang, G. Y., Zhou, L. M., Zheng, X. M., and Huang, W. D.: Temporal distribution and potential hazards of wet depostion mercury in Yangtze River Estuary, Urban Environmental & Urban Ecology, 1-4, 2010.

Zhang, H., Fu, X. W., Lin, C. J., Wang, X., and Feng, X. B.: Observation and analysis of speciated atmospheric mercury in Shangri-La, Tibetan Plateau, China, Atmospheric Chemistry and Physics, 15, 653-665, 2015.

Zhang, H., Fu, X. W., Lin, C.-J., Shang, L. H., Zhang, Y. P., Feng, X. B., and Lin, C.: Monsoon-facilitated characteristics and transport of atmospheric mercury at a high-altitude background site in southwestern China, Atmospheric Chemistry and Physics, 16, 13131-13148, 2016.

Zhang, L., Wang, S. X., Wang, L., Wu, Y., Duan, L., Wu, Q. R., Wang, F. Y., Yang, M., Yang, H., Hao, J. M., and Liu, X.: Updated emission inventories for speciated atmospheric mercury from anthropogenic sources in China, Environmental Science & Technology, 49, 3185-3194, 2015.

Zhang, L. M., Wright, L. P., and Blanchard, P.: A review of current knowledge concerning dry deposition of atmospheric mercury, Atmospheric Environment, 43, 5853-5864, 2009.

Zhang, Y. X., Jacob, D. J., Horowitz, H. M., Chen, L., Amos, H. M., Krabbenhoft, D. P., Slemr, F., St Louis, V. L., and Sunderland, E. M.: Observed decrease in atmospheric mercury explained by

global decline in anthropogenic emissions, Proceedings of the National Academy of Sciences of the United States of America, 113, 526, 2016.

Zhao, B., Wang, S. X., Liu, H., Xu, J. Y., Fu, K., Klimont, Z., Hao, J. M., He, K. B., Cofala, J., and Amann, M.: NOx emissions in China: historical trends and future perspectives, Atmospheric Chemistry and Physics, 13, 9869-9897, 2013.

Zhu, J., Wang, T., Talbot, R., Mao, H., Hall, C. B., Yang, X., Fu, C., Zhuang, B., Li, S., Han, Y., and Huang, X.: Characteristics of atmospheric total gaseous mercury (TGM) observed in urban Nanjing, China, Atmospheric Chemistry and Physics, 12, 12103-12118, 2012.

Figure citation

Figure 1. The location of the Chongming monitoring site in Shanghai, China

Figure 2. Monthly average GEM concentrations during the studied period (a) observed monthly GEM concentrations (b) GEM trend after decomposition (c) GEM seasonality after decomposition (d) GEM random after decomposition

Note: The observed concentrations during July 2015-April 2016 were TGM concentrations indeed due to the problems of Tekran 1130/1135. However, the GOM concentrations at Chongming Island accounted for less than 1% of TGM. Thus, the GEM concentrations were approximated to TGM concentrations during July 2015-April 2016.

Figure 3. Monthly variations of GEM concentration at remote sites in China

Figure 4. Seasonal cycle of GEM concentrations and emissions during 2014-2016. The error bars represent the standard deviation of seasonal average. Negative values of natural emissions represent mercury deposition and positive values of natural emissions represent natural emissions.

Figure 5. Source regions of GEM at monitoring site from PSCF model in 2014(a) and 2016(b)

Figure 6. The back trajectories map for cluster NCP, SW-YRD and ABROAD in 2014(a) and 2016(b)

(NCP – North China Plain; SW-YRD –Southwest region and Yangtze River Delta; ABROAD – Abroad)

Table citation

Table 1. PCA component loading of GEM and the co-pollutant**s**

Table 2. Main air pollutant emitted by the different sector in YRD region in 2014

Table 3. The statistics of cluster and estimated contribution of GEM reduction in 2014 and 2016

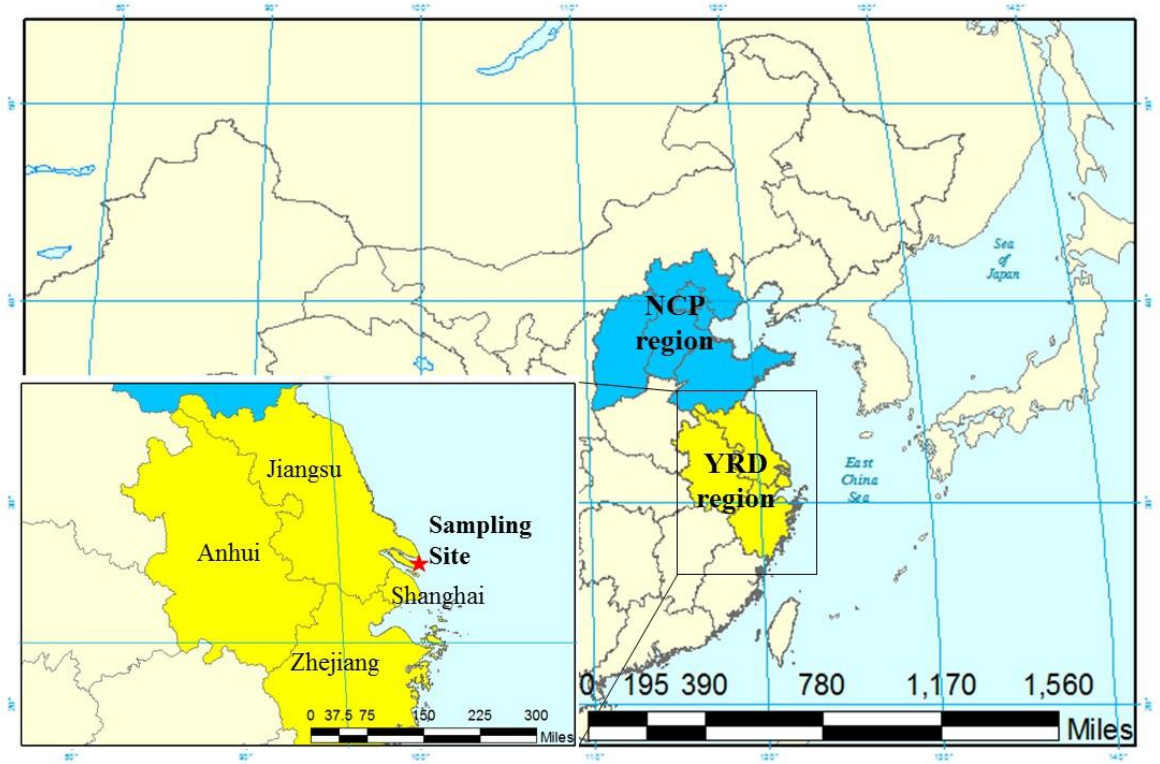

602 **Figure 1**. The location of the Chongming monitoring site in Shanghai, China

603

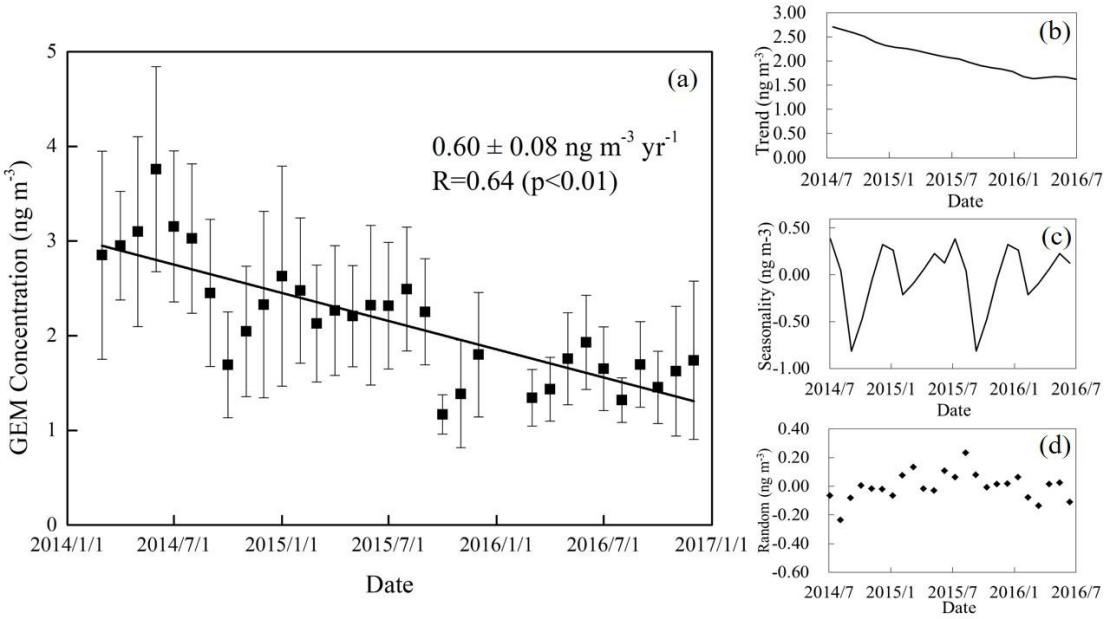

Figure 2. Monthly average GEM concentrations during the studied period (a) observed monthly GEM concentrations (b) GEM trend after decomposition (c) GEM seasonality after decomposition (d) GEM random after decomposition

Note: The observed concentrations during July 2015-April 2016 were TGM concentrations indeed due to the problems of Tekran 1130/1135. However, the GOM concentrations at Chongming Island accounted for less than 1% of TGM. Thus, the GEM concentrations were approximated to TGM concentrations during July 2015-April 2016.

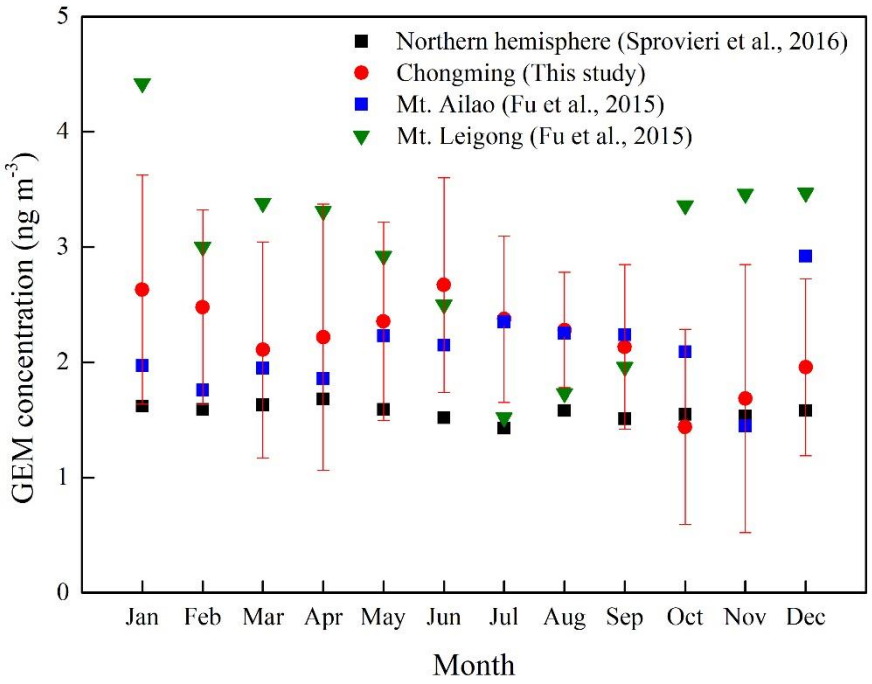

613 **Figure 3.** Monthly variations of GEM concentration at remote sites in China

614
615

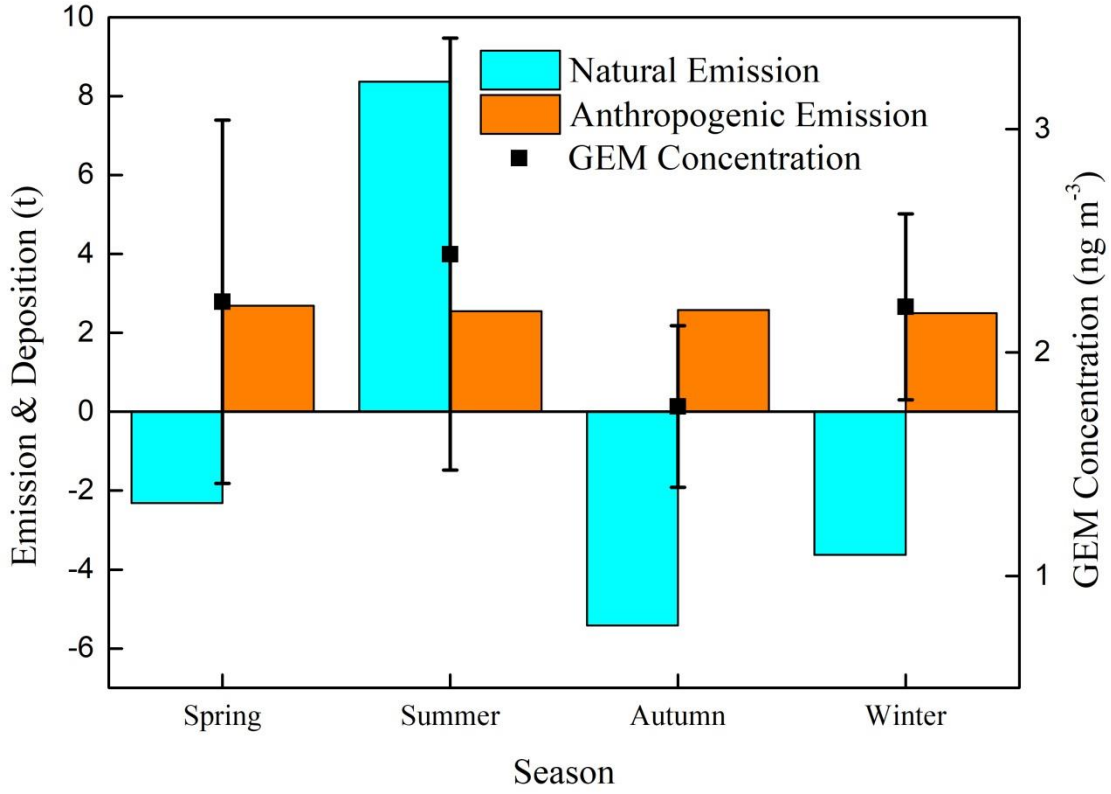

Figure 4. Seasonal cycle of GEM concentrations and natural emissions during 2014-2016. The error bars represent the standard deviation of seasonal average. Positive values of natural emissions represent Hg emitted to air. Otherwise, negative values represent Hg deposition.

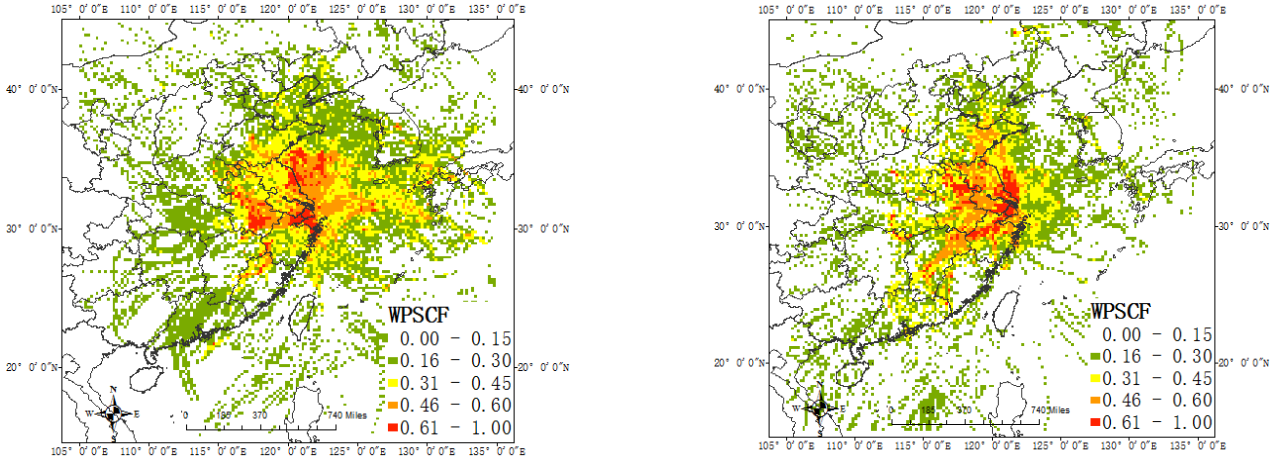

(a) 2014 (b) 2016

Figure 5. Source regions of GEM at monitoring site from PSCF model in 2014(a) and 2016(b)

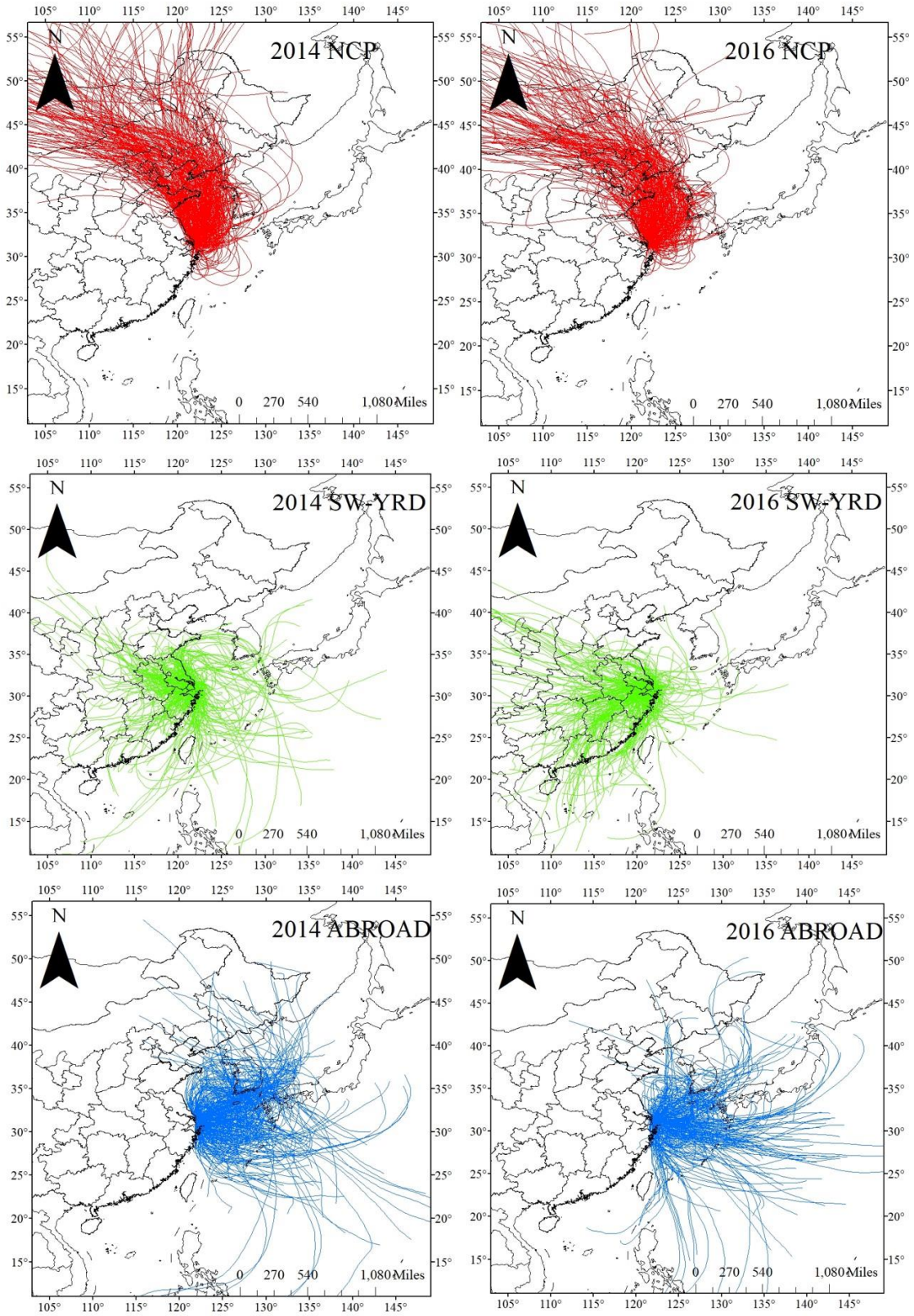

(a) 2014 (b) 2016

Figure 6. The back trajectories map for cluster NCP, SW-YRD and ABROAD in 2014(a) and 2016(b)

(NCP – North China Plain; SW-YRD –Southwest region and Yangtze River Delta; ABROAD – Abroad)

631 **Table 1**. PCA component loading of GEM and other air pollutants

Air pollutants	2014		Air pollutants	2016	
	Factor 1	Factor 2		Factor 1	Factor 2
SO_2	**0.76**	0.14	SO_2	**0.82**	-0.09
NO_X	**0.76**	-0.20	NO_X	**0.70**	**-0.52**
O_3	-0.11	**0.98**	O_3	-0.41	**0.97**
$PM_{2.5}$	**0.85**	0.05	$PM_{2.5}$	**0.88**	0.05
GEM	**0.66**	0.02	GEM	**0.78**	-0.19
CO	**0.79**	0.12			
Component	Combustion	Invasion of air mass from stratosphere	Component	Combustion	Invasion of air mass from stratosphere
Variance explain (%)	49.36	17.53	Variance explain (%)	50.63	25.10

632 Note: Text in bold phase were regarded as high loading (factor loading>0.40 or <-0.40)
633

634 **Table 2.** Emissions of the main air pollutants in YRD region in 2014

Emission sectors	Annual emissions			
	SO_2 (kt)	NO_x (kt)	$PM_{2.5}$ (kt)	GEM (t)
Coal-fired power plants	918.31	991.62	118.42	14.00
Coal-fired industrial boilers	311.03	271.94	79.91	9.80
Residential coal combustion	68.48	42.11	163.93	0.40
Cement clinker production	207.48	371.13	208.02	4.70
Iron and steel production	480.97	142.80	169.84	2.30
Mobile oil combustion	38.43	1786.74	98.00	1.90
Other sectors	348.83	316.28	382.48	2.50

635

636
637
638

639 **Table 3.** The statistics of cluster and estimated contribution of GEM reduction in 2014 and 2016

Time	Cluster	Trajectories			GEM concentration, C_j (ng m^{-3})	Trajectory weighted concentration, TWC_j,(ng m^{-3})	Contribution to GEM reduction , CR_i
		Numbers	Ratio	Average Ratio (AR)			
2014	NCP	285	33%	32%	2.33	0.79	
	SW-YRD	304	35%	37%	3.19	1.18	
	ABROAD	275	32%	31%	2.58	0.77	
2016	NCP	237	31%	32%	1.48	0.50	26%
	SW-YRD	302	39%	37%	1.87	0.69	44%
	ABROAD	230	30%	31%	1.44	0.43	30%

640